LIGO-T980129-00-D

HYTEC-TN-LIGO-36
12/29/98

HYTEC INCORPORATED

Transfer Function and Drift Measurements on the BSC First Article Stack

Eric Ponslet

December 29, 1998

Abstract

This report summarizes the results from a series of performance tests performed at HYTEC Inc. in November and December 1998, on the LIGO BSC vibration isolation stack prototype. The tests were intended to provide experimental data on stack drift and vibration isolation performance. The measured isolation performance shows exceptional agreement with computer simulations.

DESIGN ENGINEERING
ADVANCED COMPOSITE APPLICATIONS
ULTRA-STABLE PLATFORMS

110 EASTGATE DR., STE. 100
LOS ALAMOS, NM 87544

PHONE 505 661-3000
FAX 505 662-5179
WWW.HYTECINC.COM

LIGO PROJECT

Table of Contents

1. Overview

A complete first article BSC SEI system has been assembled at HYTEC for fit, function, and performance tests. The assembly includes the piers (shortened version), actuator stacks (coarse and fine), cross beams, support tubes and support platform, and the isolation stack and downtube/optics table.

The assembly is shown in Fig. 1. The figure also shows the directions of the reference axes and the 6 associated degrees of freedom: *U, V, W* (translations) and α, β, and γ (rotations).

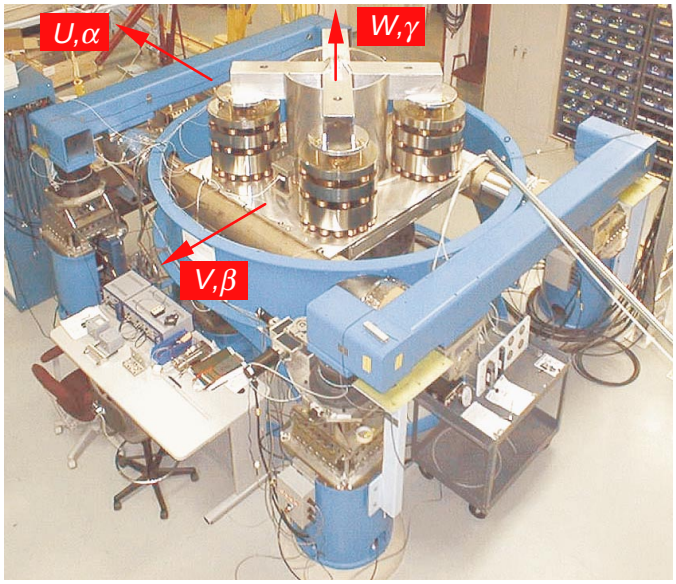

Figure 1: BSC SEI first article assembly at Hytec, Inc.

This report summarizes the results from a series of tests performed on this assembly during the end of the year 1998 and intended to evaluate the multi-stage isolation stack for viscoelastic drift rates and vibration isolation performance.

2. Creep Measurements

2.1 Stack Configuration

The stack tested for creep was the first prototype BSC stack assembled at HYTEC on November 12, 1998. The stack has an even mix of left- and right-handed coil springs at every layer of every leg. All springs in the stack were of the non-epoxied variety, except for the top stage which used epoxied springs.

At the time of these tests, the downtube was not yet equipped with a dummy payload, and was therefore missing 2224 N (500 lb) of weight. Because of this, the springs of stages 1, 2, 3, and 4 were only loaded to 92, 88, 79, and 69 %, respectively, of their nominal design load of 445 N (100 lb).

2.2 Experimental Setup

The position of the optics platform was monitored along 3 degrees of freedom: *W*, α, and β. The vertical drift *W* was measured using a Starrett digital "dial" indicator with a resolution of 1 μm. The roll and pitch angular motions were measured with an electronic level (from Applied Geomechanics, Inc.) with a resolution of 1 μradian. All data was recorded by hand.

All springs had been previously tested under nominal loads but none of the seats had been loaded prior to this test. The springs and seats were set in place while the downtube and stack elements were hanging from the overhead crane and the series of conical alignment pins. The downtube was then lowered, loading all springs in the stack within a few seconds of each other. The *W* drift recording was started within a couple seconds of the stack being fully resting on the springs. Angular motions were recorded starting 10 minutes later. Data was acquired for about 5 days, before the system had to be made available for functional tests of the coarse actuation system.

The support platform was leveled in roll and pitch.

The air temperature in the laboratory was maintained between 19.5 and 21.6 ºC throughout those tests.

2.3 Results

The measured drift components are plotted in Fig. 2 on a logarithmic time scale. The results show classic visco-elastic drift, corresponding to:

$$(d - d_0) = \nu \ln(t - t_0) \qquad (1)$$

where d and d_0 are the values of a drift degree of freedom at times t and t_o, and ν is the logarithmic drift rate. The drift rate ν can be interpreted as the amount of drift per interval of duration τ, after a length of time under load also equal to τ, for any τ. A common way of quoting drift rate is in terms of the drift per day at day 20, which is then equal to ν/20.

Figure 2 also shows the best linear fits obtained with the measured data. They correspond to:

- for W: $\nu_W/20$ = 14.7 μm/day at day 20.
- for α: $\nu_\alpha/20$ = -0.48 μrad/day at day 20.
- for β: $\nu_\beta/20$ = -0.30 μrad/day at day 20.

The W drift rate is well below the required maximum of 50 μm/day at day 20[1]; horizontal or angular requirements have not been specified. The rates measured are also not inconsistent with those measured on the HAM isolation stacks[2].

Shear drift measurements in response to angular (pitch and roll) actuation of the support table have not been performed at this time.

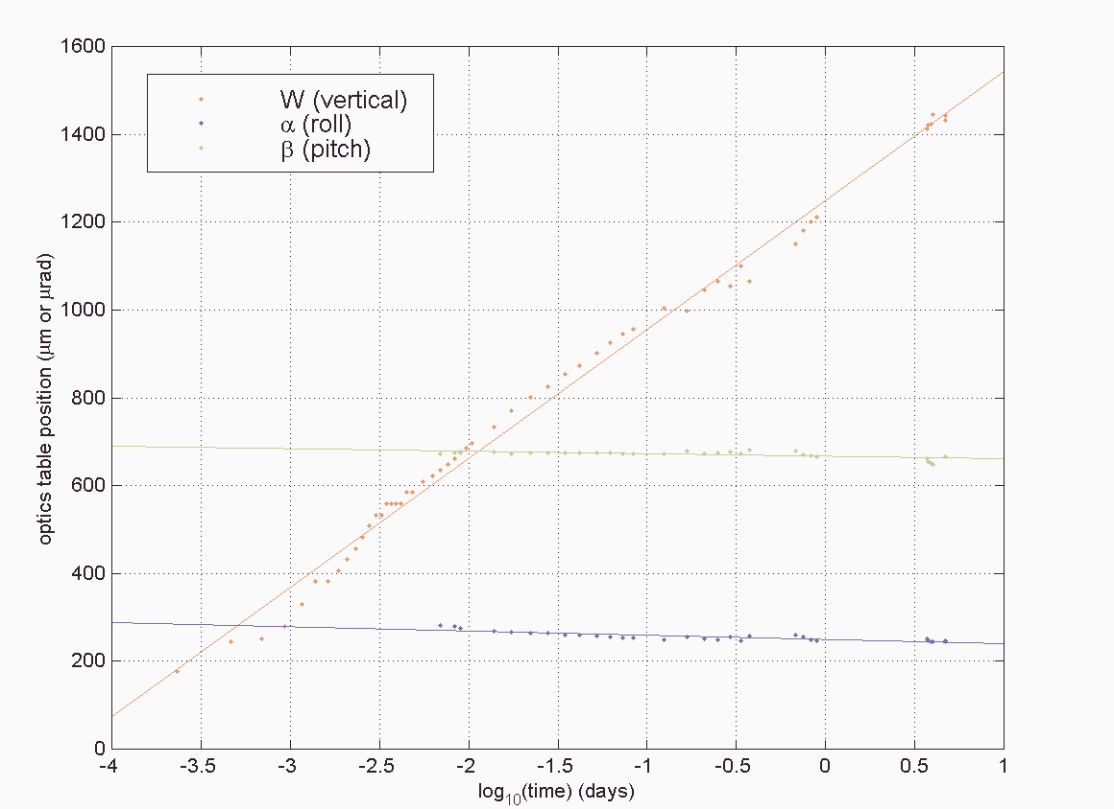

Figure 2: measured (dots) creep motions of the optics platform during the first 4 days after lowering the stack on the springs; three degrees of freedom were measured: vertical (*W*), pitch (β), and roll (α); the best linear fits are also shown (solid lines).

3. Vibration Isolation Performance Measurements

3.1 Stack Configuration

Because all springs used in the first stack (and for creep testing) had to be shipped back to LIGO, the stack had to be reassembled with different springs for the isolation performance tests. This new stack still contained an even mix of left- and right-handed springs, but this time all springs were of the epoxied variety.

A dummy payload was attached to the optics table as shown in Fig. 3. It consists of a solid 1" thick aluminum plate (86 kg or 189 lbs), 2 fine actuator stage dummies (D972107, each 64 kg or 141 lb), and 2 rectangular steel plates (each 10 kg or 23 lbs), for a total of 234 kg (516 lbs).

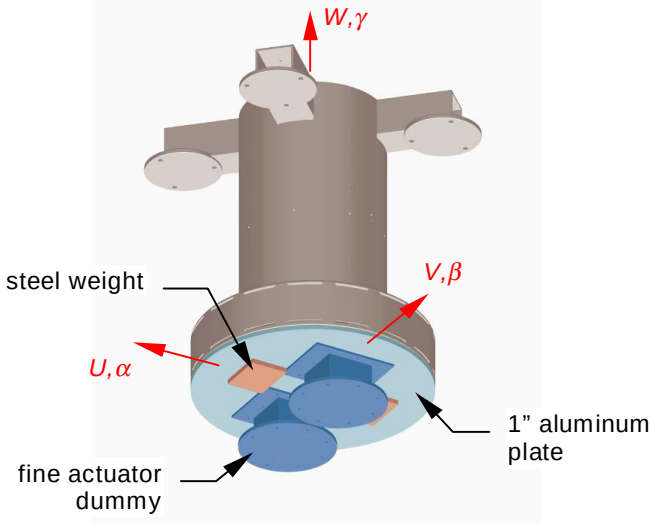

Figure 3: payload configuration used in performance tests of the BSC vibration isolation stack.

3.2 Analytical Model

Analytical predictions of support platform to optics table transmissibilities are calculated with the lumped parameter models developed early in the project for stack design purposes. Figure 4 illustrates the model.

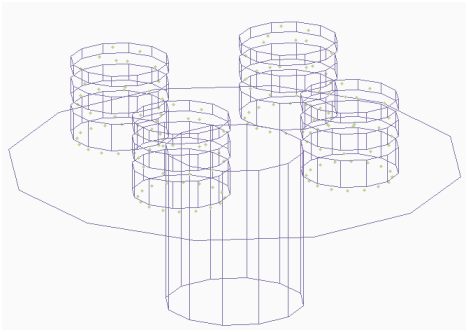

Figure 4: lumped parameter model of BSC vibration isolation stack; the model has 78 degrees of freedom.

The modeling technique is described in detail in an earlier report[3]. The spring properties used in those models are semi-empirical compilations of experimental measurements[4] and analytical predictions. The latest update of the BSC model was documented in July 1997[5]. That model was updated again to account for the actual payload used in the tests (as shown in Fig. 3).

3.3 Experimental Setup

3.3.1 Shakers

Two shaker configurations were used: one to produce horizontal motion of the support platform, and another to produce vertical motion.

For horizontal excitation, the piezo-electric stacks (PZTs) of the fine actuation stages were used as the shakers. They produce essentially pure U motion of the support platform (see Section 3.5.1), roughly proportional to the applied control voltage (18 μm/V). To achieve good response of the PZTs up to 20 Hz, the strain gage feedback controllers were disabled. This introduces a small non-linearity (hysteresis) in the voltage-displacement transfer function.

With white noise excitation in the DC to 20 Hz range, the usable RMS displacement is limited by the need to avoid inertial reactions on the fine actuator that would exceed the external preload on the PZTs and cause hammering in the ball seats that connect the PZTs to the flexure stages. An acceptable level was determined to be 0.13 V RMS or 2.3 μm RMS. This produces controlled support platform motions largely in excess of the seismic background down to about 0.4 Hz.

For vertical excitation of the support platform, two reaction mass shakers were borrowed from the PEM group. These shakers use B&K 4809 electromagnetic actuators driving suspended 8.3 kg reaction mass.

The shakers were installed on the support platform, in the *V*-*W* mid-plane, on either side of the downtube clearance hole (Fig. 5). They were driven in parallel to produce a somewhat pure vertical motion of the support platform (see Section 3.5.1).

It should be noted that the amount of vertical motion induced in the support platform with these shakers is very limited, particularly at lower frequencies; this results from a combination of factors:

- the high stiffness of the BSC support system (much stiffer than the smaller HAM structures).
- the availability of only 2 shakers (as opposed to 4 used for the HAM tests[2]).
- the limited displacement range of the shakers, which limits the amount of inertial force available at lower frequencies. Note also that using sine sweep techniques does not significantly alter this limitation, because the total peak to peak displacement during a white noise test is very strongly dominated by the lowest frequency component (since for a given force, the displacement required varies as $1/f^2$).

These limitations only allowed us to achieve a reasonable signal to noise ratio down to about 4 Hz; evidence of this can be found in the low coherence in Fig. 13, at frequencies below a few Hz.

Figure 5: prototype stack with reaction mass shakers in position on the support platform.

A configuration where the shakers are exciting the support platform directly and not via the inertia of a reaction mass may provide slightly better results at low frequencies. The shaker bodies could be attached to the BSC vacuum chamber floors or to very large reaction blocks hanging from the overhead crane. Flexible stingers would be used to connect the shaker heads to the support platform.

3.3.2 Sensors

The motions of the support platform and optics table were measured with two Integrated Dynamics TAS-3000 3 axis geophones, provided by LIGO's PEM group. They are electromagnetic velocity sensors with an advertised bandwidth of 0.08 to 100 Hz and a sensitivity of 1.0×10^5 V/m/s. With this sensitivity, residual optics table motion can easily be detected from a few tenths of a Hz to more than 20 Hz.

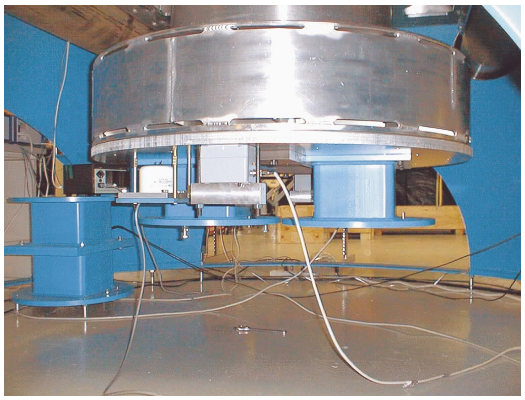

Figure 6: payload, inclinometer, and geophones attached to the BSC optics table.

3.3.3 Data Acquisition

All data acquisition and signal processing calculations were handled by an 8-input, 4-output PC controlled digital signal analyzer (2 Siglab 20-42 modules, from DSP Technology, Inc.[6]). The data acquisition and signal generation tasks are driven from a series of Matlab GUI tools. This system allowed us to acquire all 6 geophone signals and a reference signal in a single run. The data is processed internally and in real time to provide transfer and coherence functions; it is saved to disk and can later be loaded directly into Matlab for post processing and documentation.

Figure 7: the PC-based SigLab 20-42 data acquisition system.

3.4 Measurement Procedures

Only the T_{*U} and T_{*W} transfer functions were measured (i.e. optics table response to support platform *U* and *W* motions). The response to *V* motion was not measured since, in the BSC, it is identical to the response to *U* motion. The mass elements, downtube, and spring configuration are all ¼ turn periodic around the vertical axis; only the payload is not exactly symmetric but this is an artifact of the test setup and is easily accounted for in simulations.

With only 2 geophones and 8 data acquisition channels available, the necessary measurements were obtained in 8 separate runs: 2 shaker configurations and 4 sensing configurations.

The shaker configurations are:

- PZT stacks driving platform in *U*.
- reaction mass shakers driving the platform in *W*.

The sensing configurations are:

- both geophones on the support platform, in the *U*-*W* mid-plane.
- both geophones on the support platform, in the *V*-*W* mid-plane.
- both geophones on the optics table, in the *U*-*W* mid-plane.
- both geophones on the optics table, in the *V*-*W* mid-plane.

In all measurements, 7 input channels were used: the reference signal was always the control voltage applied to the input of the PZT controller or the shaker amplifiers, and the other 6 channels were measuring the 6 geophone axes.

To save time, all measurements were performed with pink noise excitation, in the 0.1 to 20 Hz range. Again, because the low frequency signal-to-noise is limited by the displacement range of the reaction mass shaker, a sine sweep test would *not* allow significantly higher energy input into the system at the low frequency edge of the band.

Becuase of this, there is no reason to expect significantly better measurements from a sine-sweep technique, only orders of magnitude longer data acquisition sessions.
The acquisition parameters were as follows:

- frequency range: 0.1 to 20 Hz
- frequency resolution: 0.1 Hz
- windowing: boxcar
- number of averages: 20
- data acquisition time: 3 ½ minutes

3.5 Post-Processing Assumptions and Experimental Justifications

3.5.1 Off Axis Motions of the Support Platform

We found that below 20 Hz, the motion of the support platform in response to either the PZT stacks or the reaction mass shakers is reasonably close to a "pure" translation in the *U* or *W* direction, respectively. Near and above 20 Hz, significant off-axis motion starts to appear, because of resonances in the support system. In addition, the geophones cannot pick up the residual motion of the optics table much above 20 Hz because of the very steep drop in transmissibility due to the multi-stage isolation. For these reasons, it was judged unnecessary to compensate the measurements for off-axis excitation of the stack; instead, the motion of the support platform was assumed 'pure' in the direction of the shaking.

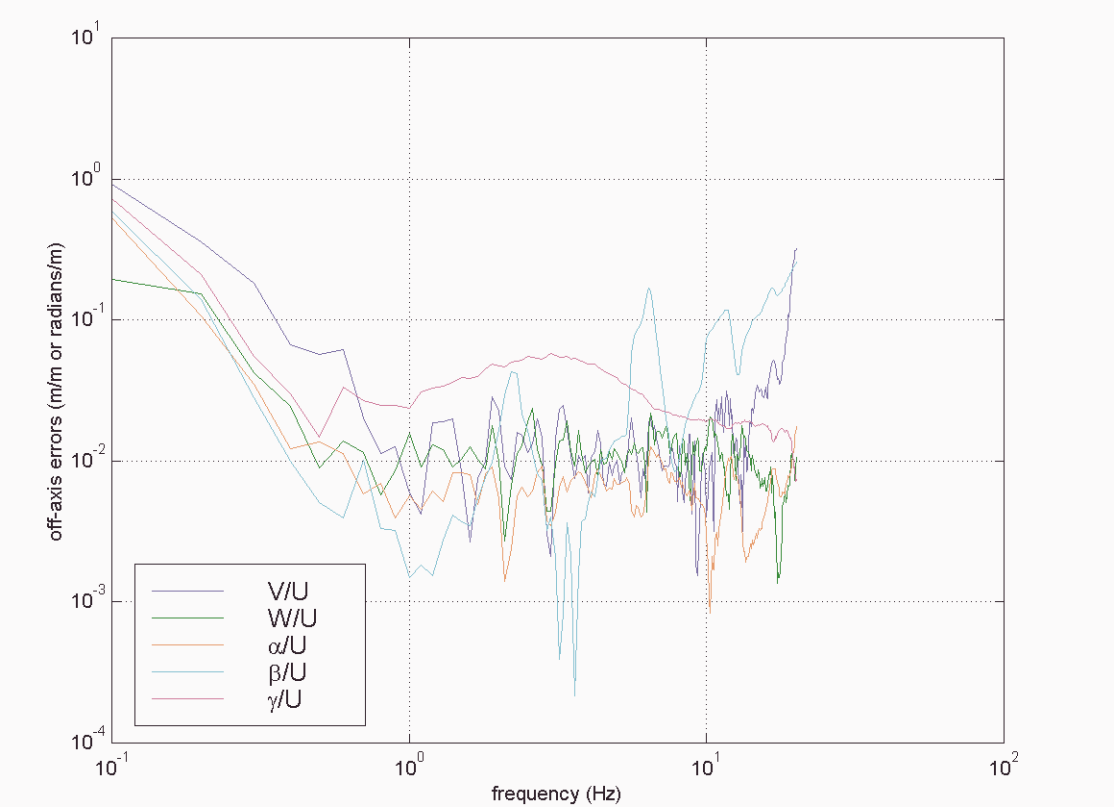

Figure 8: off-axis parasitic motions of the support platform in response to horizontal actuation by the fine stage PZT stacks.

Figure 8 shows the ratios of the off-axis motions (*V*, *W*, α, β, γ) to the primary (*U*) motion of the support platform when driven by the fine stage PZTs. All off-axis components are at about an order of magnitude smaller than the primary motion between 0.4 and 20 Hz (most are about 2 orders of magnitude smaller). Note that the apparent increase in off axis motion at frequencies below 0.4 Hz is not real but due to a very poor signal to noise ratio (seismic background becomes predominant). Above 18 Hz, off axis motion is becoming more significant because of interactions with the support system dynamics.

Similarly, Figure 9 shows the ratios of the off-axis motions (U ,V ,α ,β ,γ) to the primary (*W*) motion of the support platform when driven by the reaction mass shakers. Here, the off-axis components are negligible (about an order of magnitude smaller than the primary motion) only above 4 Hz. Below 4 Hz, the seismic background dominates the controlled motion generated by the shakers.

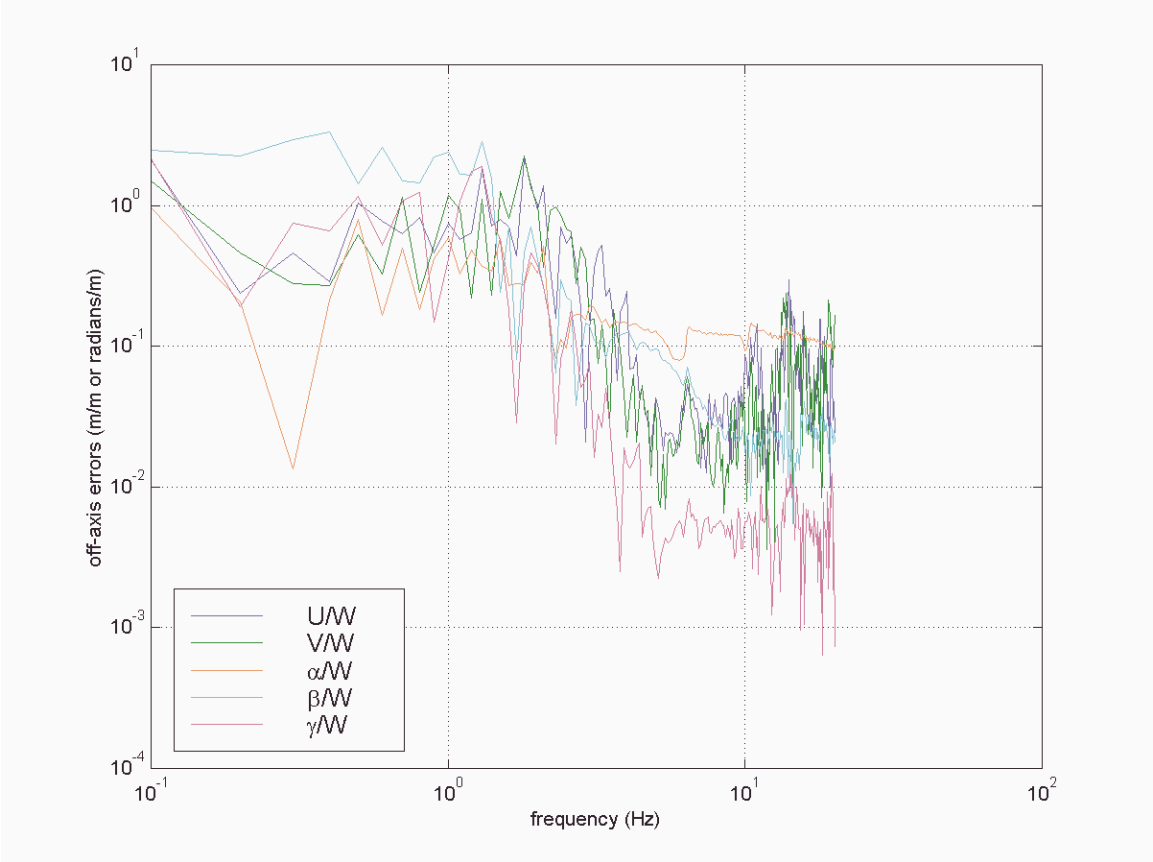

Figure 9: off-axis "parasitic" motions of the support platform in response vertical excitation by the reaction mass shakers.

3.5.2 Linear Motion Measurements

Whenever redundant measurements of a particular degree of freedom were available, the average of these spectra was retained as the final measurement.

3.5.3 Angular Motion Measurements

Angular motion measurements are obtained from the difference between the signals from both geophones, divided by the distance separating them. For such calculation to provide accurate results, and because the 6 channels of the geophones do not have identical sensitivities (magnitude and phase) across the frequency range of interest, it is essential that any difference in sensitivity be compensated for by calibration. To measure these calibration spectra, we placed both geophones next to each other, aligned along the axis to be calibrated, on the support platform excited by the PZT stacks. For each axis, the ratio of one geophone's (A) output to the other (B) was measured as a function of frequency. The magnitude of those ratios is plotted in Fig. 10. Note the significant mismatch below 5 Hz.

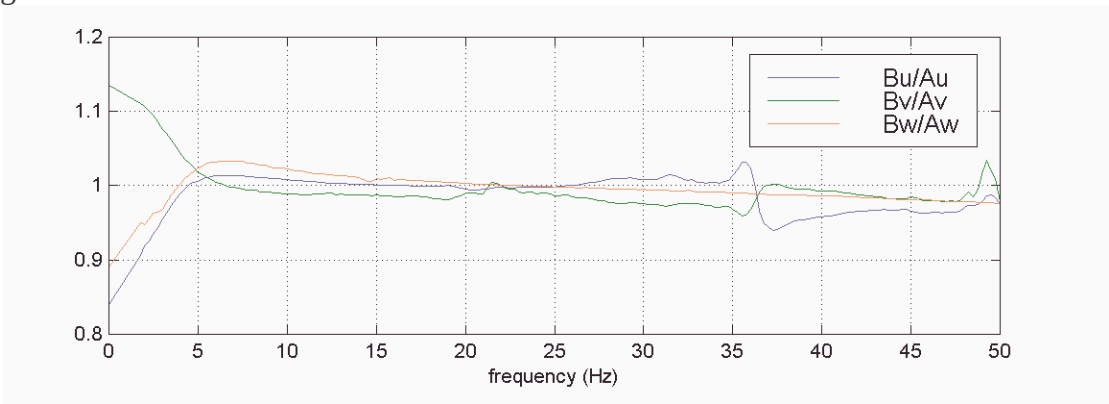

Figure 10: calibration of gain ratios of the two geophones (A and B), along the 3 sensitive axes (*u,v,w*).

3.6 Results and Comparison with Simulations

The only theoretically non-zero transfer functions that were measured are T_{UU}, $T_{\beta U}$, *and* T_{WW}. Experimental results for those components are compared to analytical predictions in the following 2 sections. Other measured components are theoretically identically zero.

3.6.1 T_{UU} and $T_{\beta U}$ (platform horizontal to optics table horizontal and pitch)

These results are plotted in Figures 11 and 12 below and compared to numerical simulations. The coherence of the measured data is also shown in the figures.
The following remarks can be made:

- overall, the analytical-experimental agreement is exceptionally good.
- for both transfer functions, the steep drop above about 15 Hz is extremely well predicted, as well as the stack modes in the 5 to 15 Hz range.
- Stack modes below 10 Hz *appear* to have higher damping (lower Q) than expected; the reason for this is not clear; it could be due to a pessimistic estimate of the springs' loss factors at lower frequencies, or to measurement errors (the coherence is very low near those resonances).

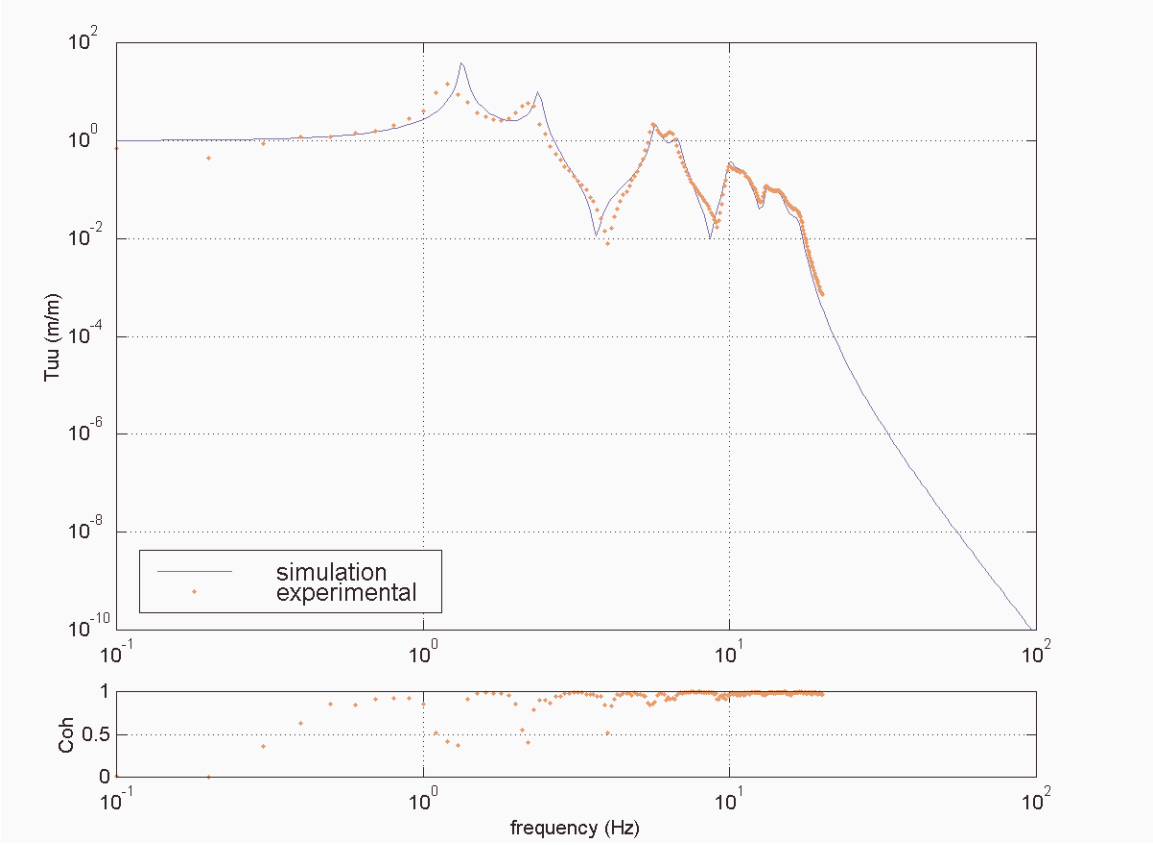

Figure 11: transfer function from horizontal motion of the support table to horizontal optics table motion; analytical and experimental results.

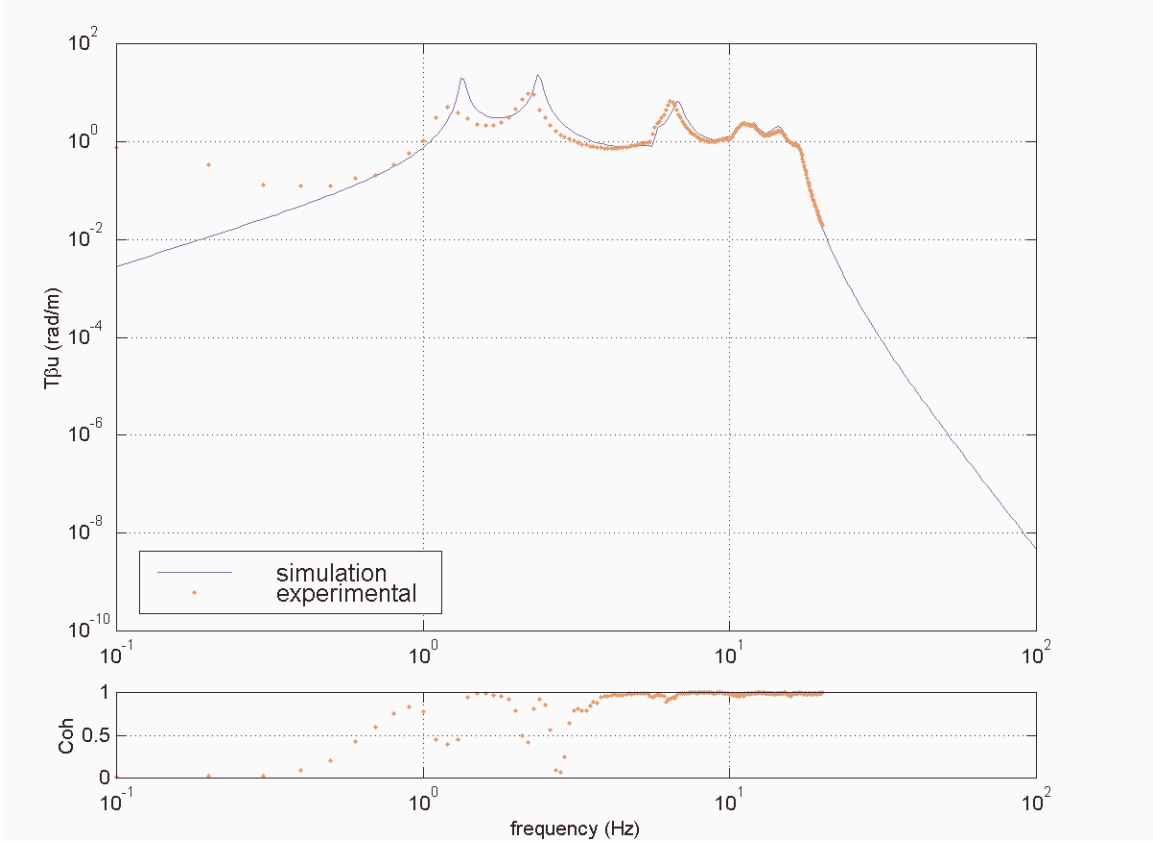

Figure 12: transfer function from horizontal motion of the support table to pitch motion of the optics table; analytical and experimental results.

3.6.2 T_{ww} (platform vertical to optics table vertical)

The measured transmissibility is plotted in Figure 13 below and compared to a numerical simulation. The coherence of the measured data is also shown in the figure.

- overall, the analytical-experimental agreement is exceptionally good.
- the steep drop above about 15 Hz is extremely well predicted, as well as the stack dynamics in the 5 to 15 Hz range.
- the lowest stack vertical mode is not accurately measured because of the poor signal to noise ratio at frequencies below 4 Hz.

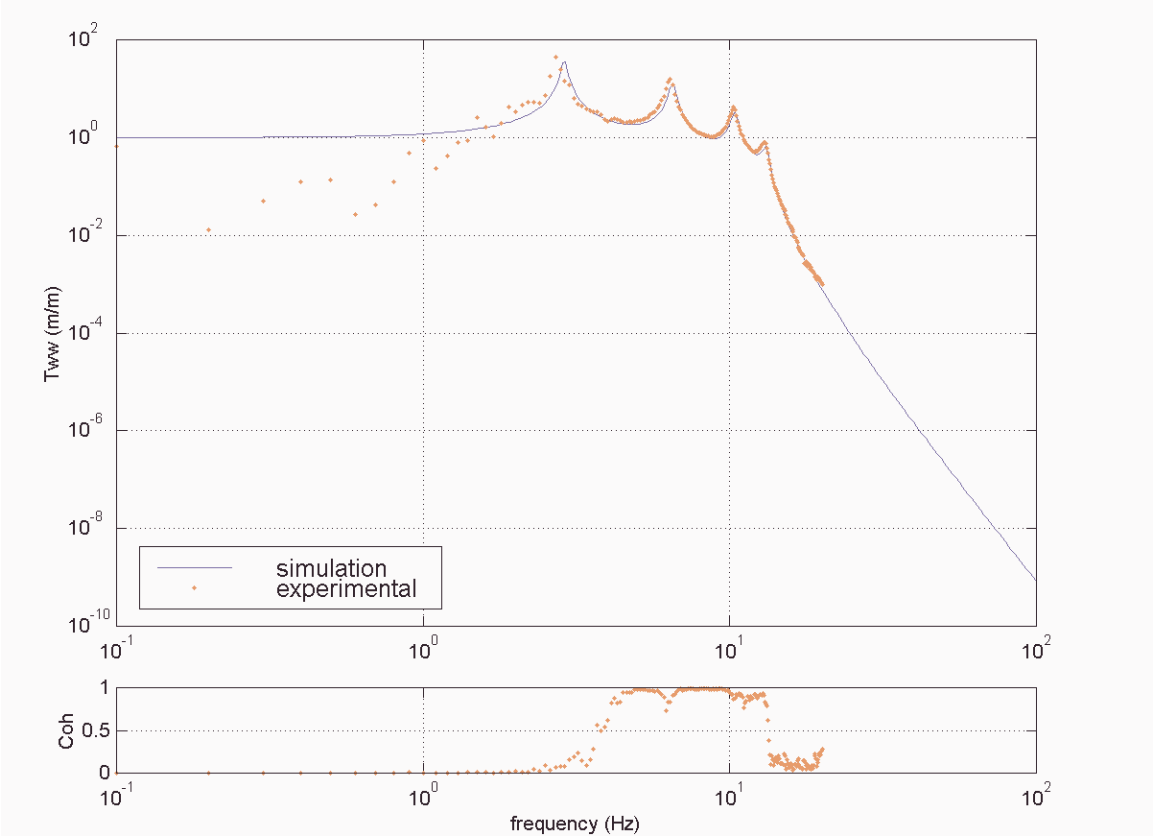

Figure 13: transfer function from vertical motion of the support table to vertical motion of the optics table; analytical and experimental results.

3.6.3 Other Components

All other components are theoretically equal to zero: the stack is symmetric, and the springs are an even mix of left- and right- handed coils. However, since the response measurements were not compensated for off axis support platform motions, the measured components are not identically zero but about an order of magnitude smaller than the primary non-zero components. Actual measurements of those other components would require complete calculation of the 6×6 matrix of transfer functions; this was not attempted.

4. Concluding Remarks

The drift characteristics of the stack on a level support platform correspond to classical visco-elastic creep. The drift rate at day 20, extrapolated from 5 days of data, is well below the LIGO requirement.

Additional drift measurements may be useful, in particular to characterize the stack for shear drift in response to a step angular perturbation of the support platform position in roll and/or pitch.

The measured stack dynamics and isolation performance is in excellent agreement with analytical predictions. Although additional measurements may be required to provide accurate information on the frequencies and quality factors of the lowest frequency stack

modes, the results presented here clearly validate the design and modeling of the isolation stack.

5. References

1. F. Raab, N. Solomonson, and M. Fine, *Seismic Isolation Design Requirements Document*, LIGO-T960065-03-D, February 20, 1997.
2. M. Barton *et al.*, *Transfer Function and Drift Measurements on the First-Article HAM*, LIGO draft document LIGO-T980084-00-D00, California Institute of Technology and Massachusetts Institute of Technology, October 9, 1998.
3. E. Ponslet, *Isolation Stack Modeling*, HYTEC Inc., Los Alamos, NM, document HYTEC-TN-LIGO-01, January 23, 1996.
4. E. Ponslet, *LIGO Coil Spring - Test Report*, HYTEC Inc., Los Alamos, NM, document HYTEC-TN-LIGO-14, February 1997.
5. E. Ponslet, *BSC Seismic Isolation with Damped Coil Springs - Performance Update*, HYTEC Inc., Los Alamos, NM, document HYTEC-TN-LIGO-20, July 26, 1997.
6. DSP Technology, Signal Analysis Group, 48500 Kato Road, Fremont, CA.

Note 1, Linda Turner, 09/03/99 03:00:07 PM
LIGO-T980129-00-D